A Bayesian Approach to Windowed DMRS Channel Estimation for Uplink MU-MIMO Systems

Jiawei Zhuang*†, Hongwei Hou*†, Minjie Tang‡, Wenjin Wang*†, Shi Jin* and Vincent K. N. Lau§
*National Mobile Communications Research Laboratory, Southeast University, Nanjing 210096, China
†Purple Mountain Laboratories, Nanjing 211100, China
‡Communication Systems Department, EURECOM, Sophia-Antipolis, France
§ Department of Electronic and Computer Engineering, Hong Kong University of Science and Technology, Hong Kong 999077, China
Email: {jw-zhuang, hongweihou, wangwj, jinshi}@seu.edu.cn, Minjie.Tang@eurecom.fr, eeknlau@ust.hk

***Abstract*—To support the increased data streams required for 6G networks, demodulation reference signals (DMRSs) from multiple users must be transmitted simultaneously on the same resource element in multi-user multiple-input multiple-output (MU-MIMO) systems. Therefore, the DMRSs of multiple users are efficiently multiplexed in the code domain via orthogonal cover code (OCC) to minimize pilot interference. In this paper, we investigate uplink DMRS-based channel estimation for MU-MIMO systems with Type II OCC pattern, leveraging statistical channel state information (SCSI) to enhance performance. Specifically, we propose a SCSI-assisted Bayesian channel estimator (SA-BCE) based on the minimum mean square error criterion to suppress the pilot interference and noise. Furthermore, we extend the SA-BCE to windowed SA-BCE (SA-WBCE) to alleviate the energy leakage caused by the limited number of subcarriers and antennas, thereby reducing computational complexity. Simulation results demonstrate that the SA-BCE and SA-WBCE significantly outperform state-of-the-art benchmarks in MU-MIMO systems.**

***Index Terms*—MU-MIMO, statistical CSI, uplink channel estimation, demodulation reference signal, windowing.**

I. Introduction

DRIVEN by the growing demand for data-hungry applications such as broadband internet of things (IoT) [1] and extended reality (XR) [2], the paradigm of uplink-centric broadband communication (UCBC), which emerged as a crucial service category in 5G-Advanced [3], now stands as a foundational requirement for the forthcoming sixth-generation (6G) networks [4]. To boost the spectral efficiency of uplink transmission, the multi-user multiple-input multiple-output (MU-MIMO) system [5] in UCBC is required to support a larger number of users transmitting data concurrently over the same resource element (RE) through spatial multiplexing. Specifically, to meet the communication requirements of more data streams in UCBC, the number of pilot ports increases from 12 to 24 in third generation partnership project (3GPP) Release 18 [6], supporting up to 24 users for uplink transmission, with a further expansion anticipated for 6G.

This work was supported in part by the National Natural Science Foundation of China under Grant 62371122, in part by the Research Grants Council of Hong Kong under Project CERG (Grant 16214122), in part by the Research Grants Council of Hong Kong under the Areas of Excellence Scheme (Grant AoE/E-101/23N), and in part by the SNS JU project 6G-GOALS under the EU's Horizon programme Grant Agreement No. 101139232.

In MU-MIMO uplink transmission, accurate channel state information (CSI) acquisition is essential for coherent detection and interference management, and is typically realized through the uplink demodulation reference signal (DMRS) [6]. In contrast to conventional channel estimation problems, DMRS-based uplink channel estimation in MU-MIMO systems poses a fundamental challenge: the pilot signals of multiple users must be transmitted simultaneously within the same RE to support the increased data streams required for 6G networks. To this end, orthogonal cover code (OCC) is typically employed to enable code-domain multiplexing, causing DMRS from different users to overlap on the same RE. Consequently, effectively decoupling these overlapping pilots via OCC decomposition becomes the first and foremost step in DMRS-based channel estimation. Several existing studies [7], [8] exploit the orthogonality of OCC under the assumption that the channel remains constant across adjacent subcarriers, thereby simplifying the decomposition process. However, in realistic frequency-selective fading environments, this assumption breaks down. The resulting loss of orthogonality among different pilot ports leads to non-negligible pilot interference, which ultimately degrades CSI estimation accuracy and constrains the spectral efficiency of MU-MIMO systems. To mitigate these issues, statistical CSI (SCSI) has emerged as a powerful tool for enhancing channel estimation performance [9]. Nevertheless, its role in assisting OCC decomposition under realistic fading conditions remains underexplored, leaving a gap in MU-MIMO uplink receiver design.

In this paper, we first develop the received signal model under the Type II OCC pattern standardized in 3GPP Release 18, which reveals the pilot interference problem in MU-MIMO uplink channel estimation. To address this challenge, we propose a SCSI-assisted Bayesian channel estimator (SA-BCE). The proposed method first applies frequency-domain minimum mean square error (MMSE) estimation to separate user signals from the superimposed received signal, followed by antenna-domain MMSE to further suppress the noise. To reduce the computational complexity, we shift from the antenna-frequency domain to the beam-delay domain and extend the SA-BCE to windowed SA-BCE (SA-WBCE).

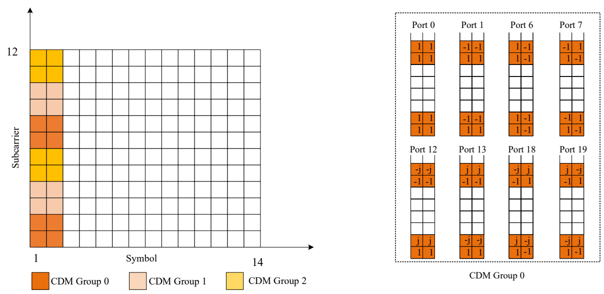

(a) (b)

Fig. 1: DMRS mapping on OFDM resource grid: (a) Type II DMRS with three CDM groups composed of 24 orthogonal pilot ports (b) OCC of CDM group 0 Type II DMRS pattern

II. System Model

We consider a single-cell massive multiple-input multiple-output orthogonal frequency-division multiplexing (MIMO-OFDM) uplink system, where the base station (BS) is equipped with a uniform planar array (UPA) with half-wavelength antenna spacing and serves K users with an omni-directional antenna. The UPA with $M = M_{\mathrm{v}} M_{\mathrm{h}}$ antennas comprises M_{v} and M_{h} antennas in vertical and horizontal directions, respectively. OFDM modulation is employed with N_{FFT} subcarriers, and the number of subcarriers for data transmission is N_{c}, with a subcarrier spacing of Δf.

A. Uplink DMRS Configuration

In the physical uplink shared channel (PUSCH), DMRS is employed to acquire CSI for subsequent coherent detection. In MU-MIMO systems, the DMRSs transmitted from different users are superimposed at the receiver. To extract individual signals from the superimposed signal, the DMRS sequence is scheduled to support multiple orthogonal ports at the transmitter. In 3GPP Release 18, Type II DMRS is specified to support a larger number of users, which divides the resource grid into multiple code division multiplexing (CDM) groups, wherein OCC are employed within each CDM group to distinguish different orthogonal pilot ports. In particular, the maximum number of orthogonal pilot ports for Type II DMRS in 3GPP Release 18 is 24, supporting up to 24 users for uplink transmission. Fig. 1 illustrates the pilot pattern of Type II DMRS in a resource block, where the pilot pattern remains consistent across all resource blocks. Within each CDM group, frequency-domain OCC and time-domain OCC are assigned to adjacent OFDM symbols to maintain orthogonality. In this pilot configuration, the number of subcarriers occupied by each CDM group is $N = \frac{N_{\mathrm{c}}}{G}$, where G represents the number of CDM groups. The number of OFDM symbols occupied by the pilots is T_{p}.

B. Signal Model

Under the aforementioned pilot configuration, the number of users in each CDM group is $\frac{K}{G}$. Without loss of generality, we assume that users with index of $\{\frac{iK}{G}+1, \frac{iK}{G}+2, ..., \frac{(i+1)K}{G}\}$ are assigned to CDM group i, where $i = 0, 1, ..., G-1$. The set of pilot subcarrier indices for CDM group i is denoted as $\mathcal{P}_i = \left\{ i+1+6\,(n-1)\,, i+2+6\,(n-1) \middle|\, n = 1, 2, \cdots, \frac{N}{2} \right\}$ [6].

Consequently, the received signal $\mathbf{Y}_i(t) \in \mathbb{C}^{N\times M}$ of CDM group i at the t-th symbol duration can be expressed as [7]

$$\mathbf{Y}_i(t) = \sum_{k=\frac{iK}{G}+1}^{\frac{(i+1)K}{G}} w_{t,k} \mathbf{S}_i \mathbf{C}_k \mathbf{H}_k^{\mathrm{PS}}(t) + \mathbf{N}(t), \tag{1}$$

where $\mathbf{H}_k^{\mathrm{PS}}(t) = \mathbf{P}_i \mathbf{H}_k(t) \in \mathbb{C}^{N\times M}$ represents frequency-space domain channel of the pilot segment for the k-th user at the t-th symbol duration, whose specific form will be discussed in Section II-C. $\mathbf{P}_i \in \{0,1\}^{N\times N_{\mathrm{c}}}$ is a sampling matrix used to select the pilot subcarrier set $\mathcal{P}_i$. $\mathbf{C}_k = \mathrm{diag}\left(1, e^{\jmath 2\pi \frac{\Delta_k}{N}} \ldots, e^{\jmath 2\pi \frac{(N-1)\Delta_k}{N}}\right) \in \mathbb{C}^{N\times N}$ represents the frequency-domain OCC of the k-th user, where $\Delta_k \in \{0, \frac{N}{4}, \frac{N}{2}, \frac{3N}{4}\}$ represents the cyclic shift of the k-th user, employed to ensure the orthogonality of the DMRS across different users. $\mathbf{S}_i = \mathrm{diag}\{\mathbf{s}_i\} \in \mathbb{C}^{N\times N}$ represents the pilot matrix of the CDM group i. Note that the power of the pilot symbols is 1, i.e., $\mathbf{S}_i \mathbf{S}_i^H = \mathbf{I}_N$. $\mathbf{N}(t) \in \mathbb{C}^{N\times M}$ is the complex Gaussian noise consisting of independently and identically distributed (i.i.d.) Gaussian variables which follow the i.i.d. complex Gaussian distribution $\mathcal{CN}(0, \sigma)$. $w_{t,k} \in \{1, -1\}$ represents the time-domain OCC of the k-th user at the t-th symbol duration, which satisfies [6]

$$\frac{1}{T_p} \sum_{t=1}^{T_p} w_{t,m} w_{t,n} = \begin{cases} 1, & \text{if } (m,n \in \mathcal{U}_1) \vee (m,n \in \mathcal{U}_2), \\ 0, & \text{otherwise}, \end{cases} \tag{2}$$

where $\mathcal{U}_1 = \{\frac{iK}{G}+1, \cdots, \frac{(2i+1)K}{2G}\}$, $\mathcal{U}_2 = \{\frac{(2i+1)K}{2G}+1, \cdots, \frac{(i+1)K}{G}\}$.

C. Channel Model

The space-frequency domain channel of k-th user at the t-th symbol duration can be modeled by [10]

$$\mathbf{H}_k(t) = \sum_{l=1}^{L_{t,k}} \alpha_{l,t,k} \mathbf{b}_{N_{\mathrm{c}}}(\tau_{l,t,k})\, \mathbf{a}(\varphi_{l,t,k}, \theta_{l,t,k})^T, \tag{3}$$

where $\mathbf{H}_k(t) \in \mathbb{C}^{N_{\mathrm{c}}\times M}$, $\mathbf{a}(\varphi_{l,t,k}, \theta_{l,t,k}) = \mathbf{a}_{\mathrm{v}}(\theta_{l,t,k}) \otimes \mathbf{a}_{\mathrm{h}}(\varphi_{l,t,k}; \theta_{l,t,k}) \in \mathbb{C}^{M\times 1}$, and $L_{t,k}$ denotes the number of multi-paths for the k-th user at the t-th symbol duration. $\alpha_{l,t,k}$, $\tau_{l,t,k}$, $\theta_{l,t,k}$, and $\varphi_{l,t,k}$ represent the complex gain, the path delay, the elevation angle of arrival (AoA), and the azimuth AoA of the l-th path for k-th user during the t-th symbol duration, respectively. $\mathbf{b}_{N_{\mathrm{c}}}(\tau) \in \mathbb{C}^{N_{\mathrm{c}}\times 1}$, $\mathbf{a}_{\mathrm{v}}(\theta) \in \mathbb{C}^{M_{\mathrm{v}}\times 1}$ and $\mathbf{a}_{\mathrm{h}}(\varphi; \theta) \in \mathbb{C}^{M_{\mathrm{h}}\times 1}$ represent the steering vectors in the delay, elevation angle and azimuth angle domains, which are defined as $[\mathbf{b}_{N_{\mathrm{c}}}(\tau)]_n = e^{-\jmath 2\pi n \Delta f \tau}$, $[\mathbf{a}_{\mathrm{v}}(\theta)]_n = e^{-\jmath \pi n \cos\theta}$ and $[\mathbf{a}_{\mathrm{h}}(\varphi, \theta)]_n = e^{-\jmath \pi n \sin\theta \cos\varphi}$, respectively.

We assume an uncorrelated fading environment, where different propagation paths are independent. Therefore, the complex gain satisfies [11]

$$\mathrm{E}\left[\alpha_{l,t,k} \alpha_{l',t,k}^*\right] = \rho_{l,t,k} \delta\left[l - l'\right], \tag{4}$$

where $\rho_{l,t,k}$ denotes the power of the l-th path for the k-th user during the t-th symbol duration.

III. SCSI-Assisted Channel Estimation

The channel estimation problem for CDM group i can be formulated as the following optimization problem:

$$\min_{\{\mathbf{H}_k(t)\}_{k=\frac{iK}{G}+1}^{\frac{(i+1)K}{G}}} \sum_{t=1}^{T_p} \left\| \mathbf{Y}_i(t) - \sum_{k=\frac{iK}{G}+1}^{\frac{(i+1)K}{G}} w_{t,k} \mathbf{S}_i \mathbf{C}_k \mathbf{H}_k^{\mathrm{PS}}(t) \right\|_{\mathrm{F}}^2 . \tag{5}$$

The number of channel parameters to be estimated in (5) is $\frac{KN_{\mathrm{c}}MT_p}{G}$, while the number of received signal is NMT_p, resulting in an under-determined estimation problem. The trivial approach [8] to solving (5) assumes that the channel coefficients remain unchanged over consecutive subcarriers, which does not hold under frequency-selective fading channels. Moreover, since the trivial approach neither incorporates inter-subcarrier nor inter-antenna correlations, its channel estimation performance deteriorates with increased pilot interference, especially in high signal-to-noise ratio (SNR) regime. To address these limitations, we first propose the SA-BCE based on the MMSE criterion. To further reduce the computational complexity, we subsequently develop SA-WBCE by incorporating the windowing technique.

A. SCSI-Assisted Bayesian Channel Estimator

As preliminary steps to the SA-BCE scheme, least squares (LS) channel estimation is first performed, followed by time-domain OCC decomposition. Specifically, the received signal $\mathbf{Y}_i(t)$ is first divided by the pilot signal $\mathbf{S}_i$ in the LS channel estimation step, i.e.,

$$\hat{\mathbf{Y}}_i^{\mathrm{LS}}(t) = \mathbf{S}_i^H \mathbf{Y}_i(t) = \sum_{k=\frac{iK}{G}+1}^{\frac{(i+1)K}{G}} w_{t,k} \mathbf{C}_k \mathbf{H}_k^{\mathrm{PS}}(t) + \mathbf{S}_i^H \mathbf{N}(t), \tag{6}$$

where $\hat{\mathbf{Y}}_i^{\mathrm{LS}}(t) \in \mathbb{C}^{N\times M}$ denotes the LS channel estimation result for the pilot segment during the t-th symbol duration.

Assuming that the channel coefficients remain constant across consecutive OFDM symbols, the effect of time-domain OCC in $\hat{\mathbf{Y}}_i^{\mathrm{LS}}(t)$ can be eliminated by exploiting its orthogonality property, as shown in equation (2), through

$$\hat{\mathbf{Y}}_i^{\mathrm{LS}} = \frac{1}{T_p} \sum_{t=1}^{T_p} w_{t,u} \hat{\mathbf{Y}}_i^{\mathrm{LS}}(t) = \sum_{k\in\mathcal{U}_1} \mathbf{C}_k \mathbf{H}_k^{\mathrm{PS}} + \mathbf{Z}, \tag{7}$$

where $u \in \mathcal{U}_1$, $\mathbf{Z} = \frac{1}{T_p}\sum_{t=1}^{T_p} w_{t,u} \mathbf{S}_i^H \mathbf{N}(t) \in \mathbb{C}^{N\times M}$.

After the time-domain OCC decoupling, the MMSE criterion is employed to decompose the frequency-domain OCC. Since the processing on different receive antennas is the same during the decomposition of the frequency-domain OCC, we omit the antenna index for convenience without loss of generality. The frequency-domain signal model after decomposing the time-domain OCC can be expressed as

$$\hat{\mathbf{y}}_i^{\mathrm{LS}} = \sum_{k=\frac{iK}{G}+1}^{\frac{(2i+1)K}{2G}} \mathbf{C}_k \mathbf{h}_k^{\mathrm{PS}} + \mathbf{z}, \tag{8}$$

where $\mathbf{h}_k^{\mathrm{PS}} \in \mathbb{C}^{N\times 1}$ represents the frequency-domain channel of the pilot segment for the k-th user. For a specific user of interest, indexed by u, the MMSE estimation of $\mathbf{h}_u^{\mathrm{PS}}$ is derived as follows [12]:

$$\hat{\mathbf{h}}_u^{\mathrm{PS}} = \mathbf{R}_{\mathbf{h}_u^{\mathrm{PS}}\hat{\mathbf{y}}_i^{\mathrm{LS}}} \mathbf{R}_{\hat{\mathbf{y}}_i^{\mathrm{LS}}\hat{\mathbf{y}}_i^{\mathrm{LS}}}^{-1} \hat{\mathbf{y}}_i^{\mathrm{LS}}, \tag{9}$$

where $\mathbf{R}_{\mathbf{h}_u^{\mathrm{PS}}\hat{\mathbf{y}}_i^{\mathrm{LS}}} = \mathbb{E}\{\mathbf{h}_u^{\mathrm{PS}} \left(\hat{\mathbf{y}}_i^{\mathrm{LS}}\right)^H\} \in \mathbb{C}^{N\times N}$ and $\mathbf{R}_{\hat{\mathbf{y}}_i^{\mathrm{LS}}\hat{\mathbf{y}}_i^{\mathrm{LS}}} = \mathbb{E}\{\hat{\mathbf{y}}_i^{\mathrm{LS}} \left(\hat{\mathbf{y}}_i^{\mathrm{LS}}\right)^H\} \in \mathbb{C}^{N\times N}$ are given by

$$\begin{aligned} \mathbf{R}_{\mathbf{h}_u^{\mathrm{PS}}\hat{\mathbf{y}}_i^{\mathrm{LS}}} &= \mathbf{P}_i \mathbf{R}_u^f \mathbf{P}_i^T \mathbf{C}_u^H, \\ \mathbf{R}_{\hat{\mathbf{y}}_i^{\mathrm{LS}}\hat{\mathbf{y}}_i^{\mathrm{LS}}} &= \sum_{k=\frac{iK}{G}+1}^{\frac{(2i+1)K}{2G}} \mathbf{C}_k \mathbf{P}_i \mathbf{R}_k^f \mathbf{P}_i^T \mathbf{C}_k^H + \sigma^2 \mathbf{I}_N, \end{aligned} \tag{10}$$

where $\mathbf{R}_k^f = \sum_{l=1}^{L_{t,k}} \rho_{l,t,k} \mathbf{b}_{N_{\mathrm{c}}}(\tau_{l,t,k})\, \mathbf{b}_{N_{\mathrm{c}}}^H(\tau_{l,t,k})$ denotes the frequency-domain channel correlations for the k-th user.

As a result, $\{\hat{\mathbf{H}}_u^{\mathrm{PS}} \in \mathbb{C}^{N\times M}\}_{u=1}^K$ can then be obtained by applying (9) to the received signals $\hat{\mathbf{y}}_i^{\mathrm{LS}}$ from all CDM groups and receive antennas, i.e.,

$$\hat{\mathbf{H}}_u^{\mathrm{PS}} = \mathbf{P}_i \mathbf{R}_u^f \mathbf{P}_i^T \mathbf{C}_u^H \Big(\sum_{k=\frac{iK}{G}+1}^{\frac{(2i+1)K}{2G}} \mathbf{C}_k \mathbf{P}_i \mathbf{R}_k^f \mathbf{P}_i^T \mathbf{C}_k^H + \sigma^2 \mathbf{I}_N \Big)^{-1} \hat{\mathbf{Y}}_i^{\mathrm{LS}}. \tag{11}$$

To further suppress the noise, we exploit the inter-antenna correlations and employ the MMSE channel estimation in the antenna domain, which gives [12]

$$(\widetilde{\mathbf{H}}_u^{\mathrm{PS}})^T = \mathbf{R}_u^s (\mathbf{R}_u^s + \sigma^2 \mathbf{I}_M)^{-1} (\hat{\mathbf{H}}_u^{\mathrm{PS}})^T, \tag{12}$$

where $\mathbf{R}_u^s = \sum_{l=1}^{L_{t,u}} \rho_{l,t,u} \mathbf{a}(\varphi_{l,t,u}, \theta_{l,t,u}) \mathbf{a}^H(\varphi_{l,t,u}, \theta_{l,t,u})$ represents the antenna-domain channel correlations for the u-th user. Finally, the full-frequency domain channel for all users, represented as $\{\hat{\mathbf{H}}_u^{\mathrm{MMSE}} \in \mathbb{C}^{N_{\mathrm{c}}\times M}\}_{u=1}^K$, is reconstructed by applying frequency-domain linear interpolation to the pilot segment channel $\{\widetilde{\mathbf{H}}_u^{\mathrm{PS}} \in \mathbb{C}^{N\times M}\}_{u=1}^K$.

B. Low-Complexity SA-BCE

The overall complexity of SA-BCE is dominated by matrix inversion with complexities of $\mathcal{O}(N^3 + M^3)$. To reduce the computational complexity of SA-BCE, we reformulate the estimation process from the antenna-frequency domain to the beam-delay domain [13] [14], thereby exploiting the limited scattering nature of wireless channels. Specifically, the beam-delay domain MMSE estimator is given by

$$\begin{aligned} \hat{\mathbf{H}}_u^{\mathrm{PS}} &= \mathbf{C}_u^H \mathbf{F}_N \mathbf{R}_u^\tau \Big(\sum_{k=\frac{iK}{G}+1}^{\frac{(2i+1)K}{2G}} \mathbf{R}_k^\tau + \sigma^2 \mathbf{I}_N \Big)^{-1} \mathbf{F}_N^H \hat{\mathbf{Y}}_i^{\mathrm{LS}}, \\ (\widetilde{\mathbf{H}}_u^{\mathrm{PS}})^T &= \mathbf{F}^A \mathbf{R}_u^a (\mathbf{R}_u^a + \sigma^2 \mathbf{I}_M)^{-1} \left(\mathbf{F}^A\right)^H (\hat{\mathbf{H}}_u^{\mathrm{PS}})^T, \end{aligned} \tag{13}$$

where $\mathbf{F}_N \in \mathbb{C}^{N\times N}$ denotes the discrete fourier transform (DFT) matrix, which is defined as $[\mathbf{F}_N]i,j \triangleq \frac{1}{\sqrt{N}} e^{-\bar{\jmath}2\pi\frac{ij}{N}}$,

$\mathbf{F}^A = (\mathbf{F}_{M_\text{v}} \otimes \mathbf{F}_{M_\text{h}}) \in \mathbb{C}^{M\times M}$. $\mathbf{R}_u^\tau \in \mathbb{C}^{N\times N}$ and $\mathbf{R}_u^a \in \mathbb{C}^{M\times M}$ denote the delay- and beam-domain channel correlations of the u-th user, respectively, and are defined as

$$\mathbf{R}_u^\tau = \mathbf{F}_N^H \mathbf{C}_u \mathbf{P}_i \mathbf{R}_u^f \mathbf{P}_i^T \mathbf{C}_u^H \mathbf{F}_N = \sum_{l=1}^{L_{t,u}} \rho_{l,t,u} \overline{\mathbf{b}}(\tau_{l,t,u}) \overline{\mathbf{b}}^H(\tau_{l,t,u}),$$
$$\mathbf{R}_u^a = (\mathbf{F}^A)^H \mathbf{R}_u^s \mathbf{F}^A = \sum_{l=1}^{L_{t,u}} \rho_{l,t,u} \overline{\mathbf{a}}(\varphi_{l,t,u}, \theta_{l,t,u}) \overline{\mathbf{a}}^H(\varphi_{l,t,u}, \theta_{l,t,u}), \tag{14}$$

where $\overline{\mathbf{b}}(\tau_{l,t,u}) = \mathbf{F}_N^H \mathbf{C}_u \mathbf{P}_i \mathbf{b}_{N_\text{c}}(\tau_{l,t,u})$, $\overline{\mathbf{a}}(\varphi_{l,t,u}, \theta_{l,t,u}) = \overline{\mathbf{a}}_\text{v}(\theta_{l,t,u}) \otimes \overline{\mathbf{a}}_\text{h}(\varphi_{l,t,u}; \theta_{l,t,u})$, $\overline{\mathbf{a}}_\text{v}(\theta_{l,t,u}) = \mathbf{F}_{M_\text{v}}^H \mathbf{a}_\text{v}(\theta_{l,t,u})$ and $\overline{\mathbf{a}}_\text{h}(\varphi_{l,t,u}; \theta_{l,t,u}) = \mathbf{F}_{M_\text{h}}^H \mathbf{a}_\text{h}(\varphi_{l,t,u}; \theta_{l,t,u})$.

Observing that the beam–delay domain MMSE estimator is equivalent to its antenna–frequency domain counterpart, we present the following lemma to establish their equivalence.

Lemma 1: The beam-delay domain MMSE estimator is equivalent to its antenna-frequency domain counterpart.

Proof: Utilizing the orthogonality property of the DFT matrix and the relation in (14), substitution of (11) and (12) directly yields the estimator in (13), thereby proving the equivalence.

Owing to the intrinsic sparsity of the beam–delay domain channel, the matrices $\mathbf{R}_u^\tau$ and $\mathbf{R}_u^a$ exhibit sparse structures, thereby enabling a significant reduction in the computational complexity. To further characterize this sparsity, we analyze the asymptotic property of $\mathbf{R}_u^\tau$ and $\mathbf{R}_u^a$, as summarized in Proposition 1.

Proposition 1: In the infinite case, $\mathbf{R}_u^\tau$ and $\mathbf{R}_u^a$ respectively converge to diagonal matrices.

Proof: In the infinite case where both the number of antennas and subcarriers tend to infinity, the sampled steering vectors exhibit asymptotic orthogonality [15], rendering $\overline{\mathbf{b}}(\tau_{l,t,u})$ and $\overline{\mathbf{a}}(\varphi_{l,t,u}, \theta_{l,t,u})$ asymptotically 1-sparse, i.e., containing only a single non-zero element. Consequently, according to (14), both $\mathbf{R}_u^\tau$ and $\mathbf{R}_u^a$ reduce to diagonal matrices in this case. This completes the proof.

Proposition 1 reveals that the beam-delay domain MMSE estimator degenerates into a element-wise operation as the number of antennas and subcarriers tends to infinity, thereby eliminating the need for matrix inversion. However, in practical systems, the number of antennas and subcarriers is finite, leading to inevitable energy leakage in the beam-delay domain. Therefore, both the beam- and delay-domain channel correlation matrices exhibit significant off-diagonal elements, which in turn substantially increases the computational complexity of the beam-delay domain MMSE estimator.

To alleviate the energy leakage problem, we incorporate the energy-concentrating property of window functions [16] into the beam-delay domain MMSE estimator to develop a windowed SA-BCE (SA-WBCE), given by

$$\check{\mathbf{H}}_u^{\text{PS}} = \mathbf{\Lambda}_f^{-1} \mathbf{C}_u^H \mathbf{F}_N \widetilde{\mathbf{R}}_u^\tau \Big(\sum_{k=\frac{iK}{G}+1}^{\frac{(2i+1)K}{2G}} \widetilde{\mathbf{R}}_k^\tau + \sigma^2 \mathbf{\Xi}_f \Big)^{-1} \mathbf{F}_N^H \mathbf{\Lambda}_f \hat{\mathbf{Y}}_i^{\text{LS}},$$
$$(\check{\mathbf{H}}_u^{\text{PS}})^T = \mathbf{\Lambda}_s^{-1} \mathbf{F}^A \widetilde{\mathbf{R}}_u^a (\widetilde{\mathbf{R}}_u^a + \sigma^2 \mathbf{\Xi}_s)^{-1} \left(\mathbf{F}^A\right)^H \mathbf{\Lambda}_s (\check{\mathbf{H}}_u^{\text{PS}})^T, \tag{15}$$

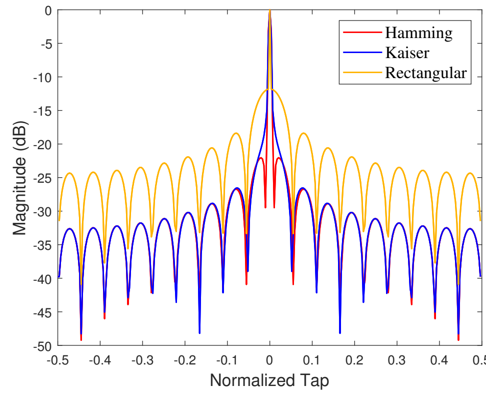

Fig. 2: The characteristics of different window functions. The shape parameter of the Kaiser window is set as 3.95.

where $\mathbf{\Xi}_f = \mathbf{F}_N^H |\mathbf{\Lambda}_f|^2 \mathbf{F}_N$, $\mathbf{\Xi}_s = \left(\mathbf{F}^A\right)^H |\mathbf{\Lambda}_s|^2 \mathbf{F}^A$, $\mathbf{\Lambda}_f \triangleq \text{diag}\{\boldsymbol{\eta}_f\} \in \mathbb{C}^{N\times N}$ and $\mathbf{\Lambda}_s \triangleq \text{diag}\{\boldsymbol{\eta}_s\} \in \mathbb{C}^{M\times M}$ denote the frequency- and antenna-domain window functions, respectively. $\widetilde{\mathbf{R}}_u^\tau \in \mathbb{C}^{N\times N}$ and $\widetilde{\mathbf{R}}_u^a \in \mathbb{C}^{M\times M}$ denote the windowed versions of the delay- and beam-domain channel correlations for the u-th user, respectively, and are given by

$$\begin{aligned}\widetilde{\mathbf{R}}_u^\tau &= \mathbf{F}_N^H \mathbf{\Lambda}_f \mathbf{C}_u \mathbf{P}_i \mathbf{R}_u^f \mathbf{P}_i^T \mathbf{C}_u^H \mathbf{\Lambda}_f^H \mathbf{F}_N \\ &= \sum_{l=1}^{L_{t,u}} \rho_{l,t,u} \widetilde{\mathbf{b}}(\tau_{l,t,u}) \widetilde{\mathbf{b}}^H(\tau_{l,t,u}), \\ \widetilde{\mathbf{R}}_u^a &= (\mathbf{F}^A)^H \mathbf{\Lambda}_s \mathbf{R}_u^s \mathbf{\Lambda}_s^H \mathbf{F}^A \\ &= \sum_{l=1}^{L_{t,u}} \rho_{l,t,u} \widetilde{\mathbf{a}}(\varphi_{l,t,u}, \theta_{l,t,u}) \widetilde{\mathbf{a}}^H(\varphi_{l,t,u}, \theta_{l,t,u}),\end{aligned} \tag{16}$$

where $\widetilde{\mathbf{b}}(\tau_{l,t,u})$ and $\widetilde{\mathbf{a}}(\varphi_{l,t,u}, \theta_{l,t,u})$ represent the windowed versions of $\overline{\mathbf{b}}(\tau_{l,t,u})$ and $\overline{\mathbf{a}}(\varphi_{l,t,u}, \theta_{l,t,u})$, respectively. Fig. 2 illustrates the characteristics of different window functions. As shown in the figure, the Kaiser and Hamming windows exhibit stronger sidelobe suppression than the rectangular window, thereby enabling $\widetilde{\mathbf{b}}(\tau_{l,t,u})$ and $\widetilde{\mathbf{a}}(\varphi_{l,t,u}, \theta_{l,t,u})$ to achieve improved energy concentration compared to $\overline{\mathbf{b}}(\tau_{l,t,u})$ and $\overline{\mathbf{a}}(\varphi_{l,t,u}, \theta_{l,t,u})$. This implies that $\widetilde{\mathbf{R}}_u^\tau$ and $\widetilde{\mathbf{R}}_u^a$ can be approximated as band matrices $\widehat{\mathbf{R}}_u^\tau$ and $\widehat{\mathbf{R}}_u^a$, i.e.,

$$\left[\widehat{\mathbf{R}}_u^\phi\right]_{i,j} = \begin{cases} \left[\widetilde{\mathbf{R}}_u^\phi\right]_{i,j}, & \text{if } |i-j| \leq B_\phi, \\ 0, & \text{otherwise}, \end{cases} \tag{17}$$

where $\phi \in \{\tau, a\}$. Due to the characteristics of the window functions, both $\mathbf{\Xi}_f$ and $\mathbf{\Xi}_s$ are band matrices with narrow bandwidths. As a result, the matrix inversion in the SA-WBCE can be simplified to the inversion of band matrices, reducing the computational complexity from $\mathcal{O}(N^3+M^3)$ to $\mathcal{O}(NB_\tau^2+MB_a^2)$.

Note that both SA-BCE and SA-WBCE rely on SCSI $\{\tau_{l,t,u}, \varphi_{l,t,u}, \theta_{l,t,u}, \rho_{l,t,u}\}_{l=1}^{L_{t,u}}$. However, in practical systems, the ideal SCSI is not known a priori and is typically obtained by estimation [9], leading to significant processing delay. To address this issue, we also develop a practical SCSI acquisition

TABLE I: Basic System Parameters

System Parameters	Value
Centering frequency f_{c}	6.7 GHz
Number of subcarriers for transmission N_{c}	816
Subcarrier spacing Δf	30 kHz
Number of CDM group G	3
Number of OFDM symbols for pilots T_{p}	2
Number of subcarriers each CDM group N	272
Number of UE K	24
Number of BS antennas $[M_{\mathrm{v}}, M_{\mathrm{h}}]$	$[4, 16]$
Delay spread	300 ns
Window function of SA-WBCE	Kaiser window
Shape parameterof the Kaiser window	3.95

approach, which leverages the intrinsic relationship between SCSI and the wireless channel's scattering characteristics. Under the principle of spatial consistency, we construct a grid-based, location-specific SCSI database by partitioning the service area of the BS into appropriately sized grids. Facilitated by the multilinear structure of wireless channels, we formulate the SCSI acquisition problem within each grid as a tensor decomposition problem, where the factor matrices are parameterized by the multi-path powers, delays, and angles. By exploiting the Vandermonde structure of the factor matrices, we employ a Vandermonde-structured tensor decomposition algorithm to acquire the SCSI within each grids. The detailed procedures of the SCSI acquisition can be found in the full version of this paper [17].

IV. Simulation Results

A. Simulation Configuration

In this section, we present simulation results to evaluate the performance of the SA-BCE and SA-WBCE. We utilize well-established QuaDRiGa model [18] to generate the channels for simulations in the 3GPP 38.901 urban macro (UMa) line-of-sight (LoS) scenario. The basic simulation parameters are presented in Table I.

B. Benchmarks and Performance Metric

To demonstrate the superiority of the proposed schemes, we compare our schemes with the following state-of-the-art algorithms:

- OMP [19]: The orthogonal matching pursuit (OMP) algorithm estimates delay-angular channel parameters by applying OMP with a pre-defined dictionary from the trivial approach results [8]. The channel is subsequently reconstructed using the estimated parameters.
- VSD [7]: The Vandermonde structured decomposition (VSD) algorithm exploits the channel's inherent Vandermonde structure, applying tensor decomposition to estimate the channel from the trivial approach results [8].
- EM-AMP [20]: This algorithm uses the expectation-maximization (EM) algorithm to learn the hyper-parameters of a Bernoulli-Gaussian prior, and then estimates the channel from the trivial approach results [8] via approximate message passing (AMP).

To assess the performance of channel estimation, we adopt the normalized mean squared error (NMSE) [9] and the average effective communication rate [5] as the performance metric.

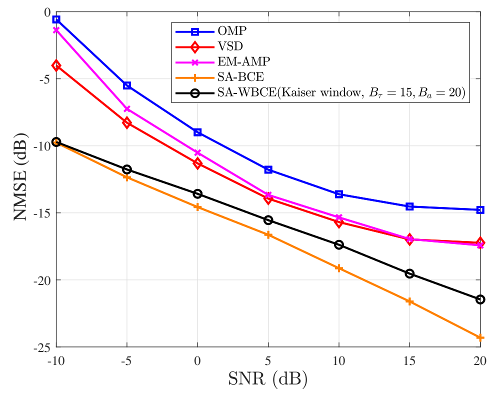

Fig. 3: The NMSE performance of channel estimation versus SNR.

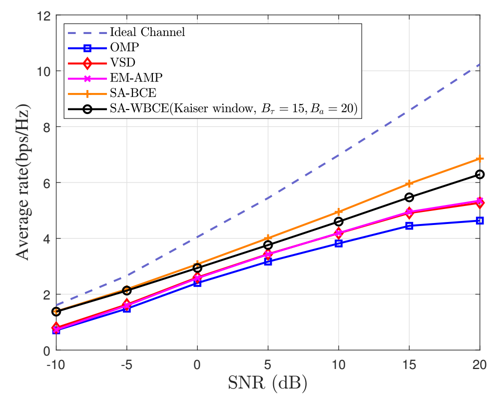

Fig. 4: Average effective communication rate performance versus SNR.

C. Performance Evaluation

The comparison of NMSE and average effective communication rate performance between the proposed schemes and baseline methods is shown in Fig. 3 and Fig. 4, respectively. By leveraging the SCSI, the proposed schemes outperform all benchmark methods across the entire SNR range. In particular, the proposed SA-BCE and SA-WBCE achieve an NMSE of approximately -21.5 dB and -19.5 dB when SNR is 15 dB, whereas the NMSE of all other benchmark methods remains above -17 dB. The SA-WBCE exhibits inferior performance compared to SA-BCE, particularly in the high-SNR regime. This result stems from the approximations made during the design process, which, in turn, contribute to a significant reduction in computational complexity.

Fig. 5 illustrates the NMSE performance of the SA-WBCE scheme under different band sizes and window functions. As the band size increases, the NMSE performance improves, albeit at the cost of higher computational complexity. In practical applications, a balance between performance and complexity can be achieved by appropriately selecting the band size. Among the three window functions considered,

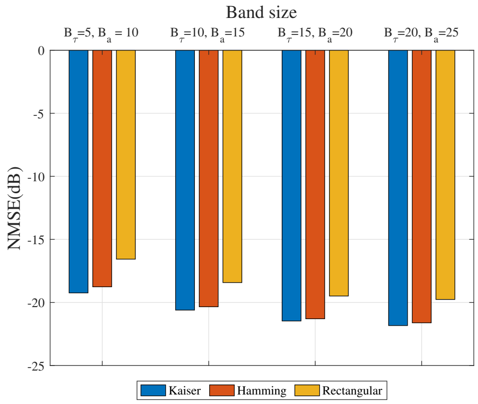

Fig. 5: The NMSE performance of SA-WBCE with different band sizes and different window functions (SNR = 20 dB).

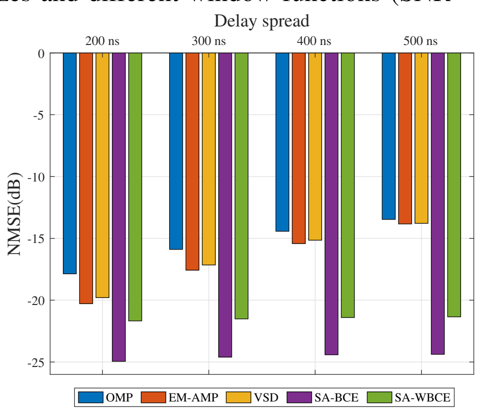

Fig. 6: The NMSE performance of various schemes versus the delay spread (SNR = 20 dB, $B_\tau = 15$ and $B_a = 20$ for SA-WBCE).

the Kaiser window offers the best performance. Specifically, when $B_\tau = 15$ and $B_a = 20$, the SA-WBCE with the Kaiser window achieves an NMSE of -21.4 dB, representing a 2 dB improvement than SA-WBCE with the rectangular window.

In Fig. 6, we present the NMSE performance of various algorithms as a function of the channel delay spread. The OMP, VSD, and EM-AMP algorithms, which rely on OCC decomposition results obtained through trivial approach [8] for channel estimation, suffer significant performance degradation as the delay spread increases. In contrast, the proposed SA-BCE and SA-WBCE, which incorporate SCSI into the OCC decomposition process to mitigate pilot interference, exhibit minimal NMSE deterioration. Specifically, as the delay spread increases from 200 ns to 500 ns, the proposed algorithms experiences only a 0.5 dB NMSE loss, compared to a 6.5 dB degradation observed in the VSD and EM-AMP algorithms.

V. Conclusion

In this paper, we investigated uplink DMRS-based channel estimation for MU-MIMO systems. We first developed the received signal model under the Type II OCC pattern. Building on this model, we proposed SA-BCE, which effectively suppresses pilot interference by fully leveraging SCSI. To further reduce the computational complexity of SA-BCE, we reformulated the estimation process from the antenna-frequency domain to the beam-delay domain and extended the SA-BCE to SA-WBCE by incorporating the windowing technique. Simulation results validated the superiority of the proposed schemes.

References

[1] H. Zhou, Y. Deng, and A. Nallanathan, "Novel listen-before-talk access scheme with adaptive backoff procedure for uplink centric broadband communication," *IEEE Internet Things J.*, vol. 10, no. 22, pp. 19 981–19 992, Nov. 2023.

[2] F. Hu, Y. Deng, H. Zhou, T. H. Jung, C.-B. Chae, and A. H. Aghvami, "A vision of an XR-aided teleoperation system toward 5G/B5G," *IEEE Commun. Mag.*, vol. 59, no. 1, pp. 34–40, Jan. 2021.

[3] W. Chen, X. Lin, J. Lee, A. Toskala, S. Sun, C. F. Chiasserini, and L. Liu, "5G-advanced toward 6G: Past, present, and future," *IEEE J. Sel. Areas Commun.*, Jun. 2023.

[4] C.-X. Wang, X. You, X. Gao, X. Zhu, Z. Li, C. Zhang, H. Wang, Y. Huang, Y. Chen, H. Haas *et al.*, "On the road to 6G: Visions, requirements, key technologies, and testbeds," *IEEE Commun. Surv. Tutor.*, vol. 25, no. 2, pp. 905–974, 2023.

[5] Y. Wang, H. Hou, X. Yi, W. Wang, and S. Jin, "Towards unified AI models for MU-MIMO communications: A tensor equivariance framework," *IEEE Trans. Wireless Commun.*, Jul. 2025, Early Access.

[6] *Physical channels and modulation, Version 18.4.0.* Standard 3GPP T.R. 38.211, Sep. 2024.

[7] P. Chen and L. Cheng, "Estimating channels with hundreds of sub-paths for MU-MIMO uplink: A structured high-rank tensor approach," *IEEE Signal Process. Lett.*, vol. 31, pp. 2320–2324, Sep. 2024.

[8] U. Mutlu and Y. Kabalci, "Deep learning aided channel estimation approach for 5G communication systems," in *2022 4th Global Power, Energy and Communication Conference (GPECOM)*. IEEE, 2022, pp. 655–660.

[9] A.-A. Lu, Y. Chen, and X. Gao, "2D beam domain statistical CSI estimation for massive MIMO uplink," *IEEE Trans. Wireless Commun.*, vol. 23, no. 1, pp. 749–761, Jan. 2023.

[10] D. Tse and P. Viswanath, *Fundamentals of wireless communication*. Cambridge university press, 2005.

[11] L. You, X. Gao, A. L. Swindlehurst, and W. Zhong, "Channel acquisition for massive MIMO-OFDM with adjustable phase shift pilots," *IEEE Trans. Signal Process.*, vol. 64, no. 6, pp. 1461–1476, Mar. 2016.

[12] S. M. Kay, "Fundamentals of statistical signal processing: Estimation theory," 1993.

[13] H. Hou, Y. Wang, Y. Zhu, X. Yi, W. Wang, D. Slock, and S. Jin, "A tensor-structured approach to dynamic channel prediction for massive MIMO systems with temporal non-stationarity," *arXiv preprint arXiv:2412.06713*, 2024.

[14] N. K. Jha, H. Guo, and V. K. N. Lau, "Bayesian deep end-to-end learning for MIMO-OFDM system with delay-domain sparse precoder," *arXiv preprint: 2504.20777*, 2025.

[15] Y. Zhu, J. Zhuang, G. Sun, H. Hou, L. You, and W. Wang, "Joint channel estimation and prediction for massive MIMO with frequency hopping sounding," *IEEE Trans. Commun.*, vol. 73, no. 7, pp. 5139–5154, Jul. 2025.

[16] C. Cai, J. Yang, F. Yang, H. Wu, and X. Gao, "Windowed information geometry approach for low-complexity channel estimation in massive MIMO-OFDM systems," *IEEE Trans. Wireless Commun.*, vol. 24, no. 1, pp. 244–259, Jan. 2025.

[17] J. Zhuang, H. Hou, M. Tang, W. Wang, S. Jin, and V. K. Lau, "DMRS-based uplink channel estimation for MU-MIMO systems with location-specific SCSI acquisition," *arXiv preprint arXiv:2506.11899*, 2025.

[18] S. Jaeckel, L. Raschkowski, K. Börner, and L. Thiele, "QuaDRiGa: A 3-D multi-cell channel model with time evolution for enabling virtual field trials," *IEEE Trans. Antennas Propagat.*, vol. 62, no. 6, pp. 3242–3256, Jun. 2014.

[19] J. A. Tropp and A. C. Gilbert, "Signal recovery from random measurements via orthogonal matching pursuit," *IEEE Trans. Inf. Theory*, vol. 53, no. 12, pp. 4655–4666, Dec. 2007.

[20] J. P. Vila and P. Schniter, "Expectation-maximization gaussian-mixture approximate message passing," *IEEE Trans. Signal Process.*, vol. 61, no. 19, pp. 4658–4672, Oct. 2013.